Angular Distribution of Gamma Rays Following Coulomb Excitation in Even-Even Nuclei

F. K. McGowan and P. H. Stelson
Oak Ridge National Laboratory, Oak Ridge, Tennessee
(Received January 7, 1957)

The angular distributions of gamma radiation from Coulomb excitation with respect to the incident proton beam on thick targets have been measured in the even-even nuclei Ru^{104}, Pd^{108}, Pd^{110}, Cd^{110}, Cd^{112}, Cd^{114}, Cd^{116}, $Os^{190,192}$, and Pt^{194}. The particle parameters a_ν for a thick target deduced from the measurements on Ru^{104}, Pd^{110}, Cd^{114}, and Pt^{194} agree to within the accuracy of the experiments (± 2 to 5% for a_2) with the numerical results from the quantum-mechanical treatment of the Coulomb excitation process.

I. INTRODUCTION

THE angular distribution of gamma radiation from Coulomb excitation with respect to the incident particles is given by

$$W(\theta)=1+\sum_\nu A_\nu a_\nu P_\nu(\cos\theta). \quad (1)$$

The coefficients A_ν are the gamma-gamma directional correlation coefficients tabulated by Biedenharn and Rose[1] for the spin sequence $j_1(L_1)j(L_2)j_2$ and the j's are the spins of the target nucleus, the Coulomb excited state, and the final state after gamma-ray emission, respectively. The particle parameters a_ν depend on the excitation process and it is the comparison of these coefficients, calculated from theory and measured by experiment, which is of interest. These coefficients were first evaluated by numerical methods for electric quadrupole excitation, using classical trajectories, by Alder and Winther.[2]

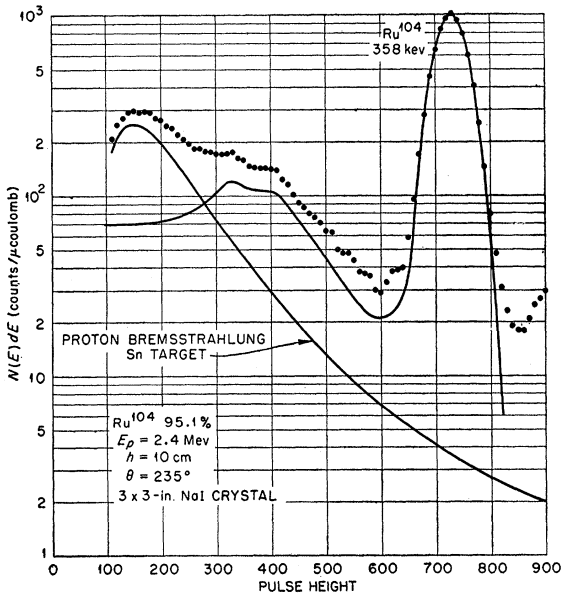

FIG. 1. Differential pulse-height spectrum of the gamma radiation for proton bombardment of Ru^{104}.

To test their numerical results, the angular distribution of gamma rays from Coulomb-excited states of spin 2 were examined and the results from these measurements have been discussed in previous papers.[3,4] The spin sequence $0(E2)2(E2)0$ is particularly suitable because the coefficients A_ν are large. In addition the reduced transition probabilities are large and no observable influence of extra nuclear fields on the angular distribution is expected. This point is important for proton-gamma angular distribution measurements where a target in the solid state is necessary. These original measurements of the particle parameters deviated considerably from the semiclassical results given by Alder and Winther. This disagreement of the particle parameters with experiment pointed to the need for a quantum-mechanical treatment of the process. Recently, numerical results from the exact treatment have been given by several groups of workers.[5-7] Both Breit and Biedenharn found an error of sign in the original calculations by Alder and Winther. As a result, a correct semiclassical calculation of the particle parameters improves the agreement with experiment regarding the slope of the a_2 *vs* E_p curve. We wish to report additional measurements of the particle parameters deduced from angular distribution measurements of gamma rays in even-even nuclei.[8] To within the accuracy of the experiments, the experimental particle parameters a_ν agree with the numerical results from a quantum-mechanical treatment.

II. APPARATUS AND METHOD

Protons of variable energy were obtained from the 5.5-million-volt ORNL Van de Graaff accelerator.

[1] L. C. Biedenharn and M. E. Rose, Revs. Modern Phys. **25**, 729 (1953).
[2] K. Alder and A. Winther, Phys. Rev. **91**, 1578 (1953).
[3] P. H. Stelson and F. K. McGowan, Phys. Rev. **98**, 249(A) (1955).
[4] F. K. McGowan and P. H. Stelson, Phys. Rev. **99**, 127 (1955).
[5] Goldstein, McHale, Thaler, and Biedenharn, Phys. Rev. **100**, 436 (1955); Biedenharn, Goldstein, McHale, and Thaler, Phys. Rev. **101**, 662 (1956).
[6] Breit, Ebel, and Benedict, Phys. Rev. **100**, 429 (1955); F. D. Benedict and G. Tice, Phys. Rev. **100**, 1545 (1955); F. D. Benedict, Phys. Rev. **101**, 178 (1956).
[7] K. Alder and A. Winther, Kgl. Danske Videnskab. Selskab, Mat.-fys. Medd. **29**, No. 19 (1955).
[8] A brief account of these measurements was presented at the 1956 Washington Meeting of the American Physical Society: McGowan, Stelson, and Bretscher, Bull. Am. Phys. Soc. Ser. II, **1**, 164 (1956).

TABLE I. Isotopic analysis of the enriched targets along with the energy (in kev) of the 2+ level in the even-even nuclei.

Target	Isotopic abundance[a] and energy of 2+ level					
Ru^{104} 95.1% 358 kev	Ru^{96} 0.2% 840	Ru^{98} 0.1% 654	Ru^{100} 0.6% 540	Ru^{102} 2.8% 475	Ru^{99} 0.5%	Ru^{101} 0.7%
Pd^{110} 91.42% 374	Pd^{104} 0.1% 555	Pd^{106} 0.86% 513	Pd^{108} 7.28% 433	Pd^{105} 0.35%		
Cd^{114} 94.2% 555	Cd^{110} 0.3% 656	Cd^{112} 2.0% 610	Cd^{116} 1.2% 517	Cd^{111} 0.4%	Cd^{113} 2.0%	
Pt^{194} 65.05% 330	Pd^{192} 0.16% 316	Pt^{196} 5.77% 358	Pt^{198} 0.42% 403	Pt^{195} 28.6%		

[a] The enriched isotopes and the isotopic analysis were supplied by the Stable Isotopes Research and Production Division at ORNL. The isotopic abundance is atomic percent.

Targets were mounted on the target support at 45° with respect to the incident ion beam. The target support was a stainless steel tube with 0.005-in. wall thickness. Metallic targets were prepared either by electrodeposition onto 0.005-in. nickel or by sintering metallic powders into thin foils 0.5 inch in diameter by 75 to 150 mg/cm² thick. When using enriched isotopes, approximately 75 to 150 mg of the enriched metal was required for each target. Targets of the normal element of Sn and Bi were electrodeposited from a sodium stannate and a bismuth perchlorate bath, respectively. The cadmium target enriched in Cd^{114} was electrodeposited from a cadmium cyanide bath to 95% depletion with a platinum anode. Targets enriched in Ru^{104}, Pd^{110}, and Pt^{194} were prepared from the metallic powders sintered at room temperature under a pressure of 25 tons/sq in. These foils were spot-welded onto 0.005-in. nickel. In Table I the isotopic analysis of each enriched target is listed along with the energy in kev of the 2+ level in the even-even nuclei.

The gamma-ray detector was a thallium-activated NaI crystal, 3 in. in diameter and 3 in. long, mounted on a DuMont type 6393 photomultiplier tube. In all angular distribution measurements the front face of the crystal was located at 20 cm from the target. To suppress the characteristic K x-rays from the target produced by the impinging protons by factors of 10^2 to 10^3, a graded shield was placed in front of the NaI detector. For example, when bombarding a cadmium target, a shield of 3.5 mils Mo and 5 mils Cu was used. The pulse-height spectrum from the detector was measured with a 20- by 120-channel analyzer.[9] Angular distributions were taken in the quadrant 0° to 90° at

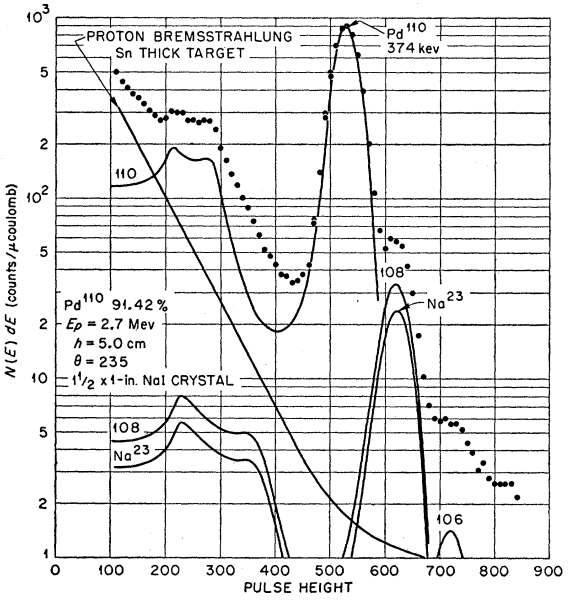

FIG. 2. Differential pulse-height spectrum of the gamma radiation for proton bombardment of Pd^{110}.

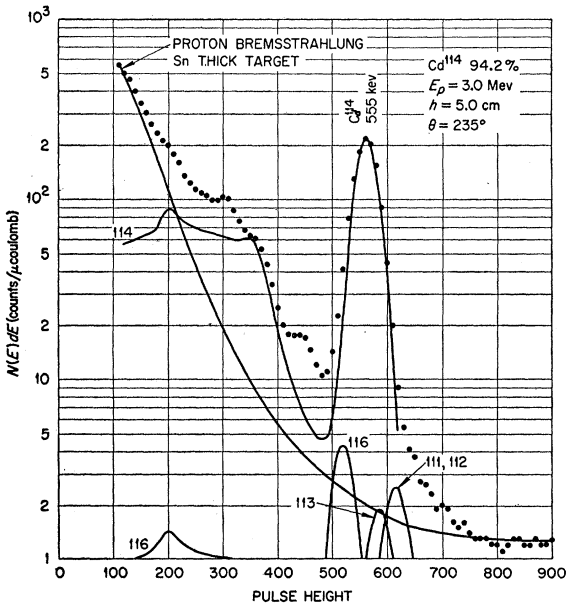

FIG. 3. Differential pulse-height spectrum of the gamma radiation for proton bombardment of Cd^{114}.

[9] Kelley, Bell, and Goss, Oak Ridge National Laboratory Physics Division Quarterly Progress Report ORNL-1278, 1951 (unpublished).

TABLE II. Proton-gamma angular distribution coefficients of the terms in the expansion of the correlation function in Legendre polynomials for a thick target. The column headed E_p gives the incident proton energy in Mev. For the spin sequence $0(E2)2(E2)0$, $A_2=0.3571$ and $A_4=1.143$.

Nucleus	E_γ (kev)	E_p (Mev)	$(a_2A_2)_{exp}$	$(a_2)_{exp}$	$(a_4A_4)_{exp}$	$(a_4)_{exp}$
$_{44}Ru^{104}$	358	1.5	0.355±0.014	0.995±0.038	−0.125±0.017	−0.110±0.015
		1.7	0.346±0.009	0.968±0.026	−0.117±0.012	−0.102±0.010
		1.9	0.294±0.006	0.824±0.016	−0.058±0.006	−0.051±0.006
		2.1	0.309±0.004	0.865±0.011	−0.092±0.003	−0.081±0.003
		2.4	0.273±0.004	0.764±0.012	−0.059±0.004	−0.051±0.004
		2.7	0.285±0.010	0.797±0.028	−0.057±0.013	−0.050±0.011
		3.0	0.237±0.009	0.663±0.025	+0.001±0.011	+0.001±0.010
$_{46}Pd^{110}$	374	1.5	0.356±0.015	0.996±0.041	−0.161±0.019	−0.140±0.017
		1.7	0.348±0.006	0.974±0.017	−0.129±0.007	−0.113±0.006
		1.9	0.319±0.005	0.893±0.014	−0.099±0.005	−0.086±0.005
		2.1	0.322±0.005	0.900±0.014	−0.095±0.005	−0.083±0.005
		2.4	0.287±0.005	0.804±0.014	−0.069±0.005	−0.061±0.005
		2.4	0.285±0.004	0.798±0.010	−0.063±0.003	−0.055±0.003
		2.7	0.271±0.006	0.759±0.018	−0.034±0.008	−0.030±0.007
		3.0	0.244±0.004	0.683±0.011	−0.038±0.003	−0.034±0.003
		3.3	0.225±0.004	0.630±0.010	−0.020±0.003	−0.018±0.003
$_{48}Cd^{114}$	555	1.9	0.411±0.010	1.151±0.027	−0.208±0.012	−0.182±0.011
		2.1	0.352±0.008	0.986±0.023	−0.117±0.010	−0.102±0.009
		2.1	0.395±0.007	1.108±0.018	−0.158±0.008	−0.138±0.007
		2.4	0.348±0.006	0.974±0.018	−0.129±0.008	−0.112±0.007
		2.4	0.357±0.005	0.999±0.014	−0.135±0.005	−0.118±0.005
		2.7	0.326±0.005	0.913±0.015	−0.095±0.006	−0.083±0.006
		2.7	0.320±0.005	0.895±0.015	−0.102±0.006	−0.089±0.006
		3.0	0.314±0.005	0.879±0.013	−0.089±0.005	−0.078±0.004
		3.0	0.286±0.007	0.801±0.020	−0.070±0.009	−0.061±0.009
		3.0	0.296±0.004	0.829±0.012	−0.090±0.004	−0.078±0.004
		3.3	0.294±0.004	0.822±0.011	−0.061±0.004	−0.053±0.004
		3.3	0.289±0.004	0.809±0.012	−0.071±0.004	−0.062±0.004
$_{78}Pt^{194}$	330	2.1	0.346±0.007	0.968±0.018	−0.123±0.008	−0.107±0.007
		2.4	0.301±0.012	0.842±0.032	−0.052±0.015	−0.046±0.013
		2.7	0.292±0.004	0.817±0.011	−0.077±0.003	−0.068±0.003
		3.0	0.272±0.004	0.762±0.011	−0.050±0.004	−0.044±0.003
		3.5	0.253±0.005	0.701±0.013	−0.019±0.005	−0.017±0.005
		4.0	0.226±0.004	0.634±0.011	−0.021±0.003	−0.019±0.003
		4.5	0.206±0.005	0.578±0.013	−0.004±0.005	−0.003±0.005
		5.0	0.192±0.006	0.538±0.016	−0.006±0.006	−0.005±0.006

10° increments where θ_i is measured with respect to the forward direction of the incident ion beam.

Because the counting rates are reasonably high and the background quite low, it is found, in practice, that the limitation to the accuracy with which the angular distributions may be determined is set by uncertainties in the alignment of the detector with respect to the source. The important error in the alignment is the determination of the position at which the proton beam strikes the target. It is believed that the position was determined to within 0.05 cm. The use of large crystals at correspondingly large distances has helped to reduce the contribution of this error. When the point at which the proton beam hit the target had been located, a

TABLE III. Angular distribution coefficients obtained from gamma-ray distribution measurements for a few other even-even nuclei.

Nucleus	E_γ (kev)	E_p (Mev)	ξ_i	$(a_2A_2)_{exp}$	$(A_2)_{exp}$	$(a_4A_4)_{exp}$
$_{46}Pd^{108}$	433	3.3	0.293	0.257±0.005	0.362±0.010	−0.047±0.005
		3.0	0.342	0.277±0.004	0.364±0.010	−0.063±0.004
		2.7	0.406	0.288±0.005	0.353±0.010	−0.067±0.005
$_{48}Cd^{116}$	517	3.0	0.438	0.251±0.010	0.300±0.02	−0.058±0.015
$_{48}Cd^{112}$	610	3.3	0.452	0.281±0.010	0.330±0.02	−0.078±0.015
		3.0	0.532	0.303±0.010	0.330±0.02	−0.101±0.015
$_{48}Cd^{110}$	656	3.3	0.494	0.276±0.010	0.310±0.02	−0.085±0.015
		3.0	0.581	0.317±0.011	0.340±0.02	−0.109±0.015
$_{76}Os^{190,192}$	186 206	3.0	0.226 0.252	0.190±0.004	0.330±0.015	−0.001±0.003

source of Cs^{137} of the same area as the beam was placed on the target at this position. Then, the axis of rotation of the detector was adjusted until the counting rates showed that the variation in the solid angle subtended by the detector at 7.5 cm from the target as a function of angular position was less than 0.5% (giving 0.1% at 20 cm from the target).

For a typical measurement the pulse-height spectrum of the full energy peak was displayed in 20 channels and ~50 000 counts were collected at each of the 10 angles. A sum of the counts in an appropriate number of channels was taken as a measure of the intensity. In all cases the intensities have been corrected for the bremmstrahlung continuum and local background by measuring the intensity of the bremsstrahlung as a function of θ_i with the same beam current. For angular distribution measurements with $Z=78$ a Bi target was used, and for measurements with Z of 44 to 48 a Sn target was used. These targets are well suited for this purpose because of the negligible yield of nuclear gamma rays from Coulomb excitation at the energies which these measurements were done. We believe the extrapolation to neighboring Z will give little error since our investigations of the bremsstrahlung process show relatively little change in character with a small change in Z.[10] In general for the measurements to be discussed below, the intensity of the bremsstrahlung in the angular distributions was never more than a few percent of the gamma-ray intensity from Coulomb excitation. Finally, a correction for the attenuation of the gamma rays in the target and target backing as a function of θ_i was applied to the observed intensities. For example, this correction, which is largest at 0° and 90°, was 0.62% for the 374-kev gamma ray from Pd^{110}. A least-squares fit of the corrected intensities (with the appropriate weight factors) in terms of a series of Legendre polynomials

$$W(\theta)=\mathfrak{A}_0'+\mathfrak{A}_2'P_2(\cos\theta)+\mathfrak{A}_4'P_4(\cos\theta) \qquad (2)$$

was carried out on an I.B.M. calculator. The standard deviations have been obtained from Eq. (30) in a paper by Rose.[11] The values of ϵ^2 defined by Eq. (27) of reference 11 clustered about unity indicating that nonstatistical errors were not large. A least-squares fit of each set of data in terms of a series of $\cos^{2n}\theta$ was carried out to serve as a check on the I.B.M. calculations.

III. GAMMA RAY SPECTRA AND MEASUREMENTS

Figures 1 to 3 show the differential pulse-height spectrum of the gamma radiation observed when thick targets of Ru^{104}, Pd^{110}, and Cd^{114} were bombarded by protons. The spectrum of the accompanying proton bremsstrahlung continuum and local background is also shown. The shape of the pulse-height spectrum for each gamma ray of discrete energy is indicated in each figure.

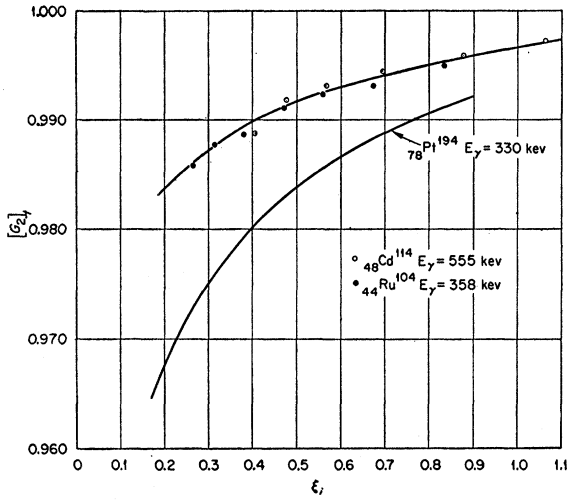

FIG. 4. The effective attenuation coefficient $[G_2]_t$ for multiple Rutherford scattering as a function of ξ_i for a few representative cases.

The pulse-height spectrum of the gamma radiation from normal platinum has been shown in a previous paper.[10] The spectrum from the target enriched in Pt^{194}

TABLE IV. Thick-target particle parameters $[a_\nu]_t$ and attenuation coefficients $[G_\nu]_t$ for multiple Rutherford scattering as given by Eqs. (3) and (5), respectively.

Nucleus	ΔE (kev)	E_i (Mev)	ξ_i	$[a_2]_t$	$[a_4]_t$	$[G_2]_t$	$[G_4]_t$
$_{44}Ru^{104}$	358	1.5	0.834	1.016	−0.122	0.9950	0.9846
		1.7	0.673	0.968	−0.101	0.9931	0.9804
		1.9	0.558	0.917	−0.0827	0.9923	0.9726
		2.1	0.472	0.869	−0.0671	0.9911	0.9667
		2.4	0.379	0.804	−0.0479	0.9887	0.9566
		2.7	0.313	0.743	−0.0323	0.9877	0.9438
		3.0	0.265	0.689	−0.0203	0.9858	0.9239
$_{46}Pd^{110}$	374	1.5	0.924	1.036	−0.132		
		1.7	0.757	0.989	−0.111		
		1.9	0.616	0.939	−0.0917		
		2.1	0.521	0.893	−0.0750		
		2.4	0.417	0.829	−0.0551		
		2.7	0.344	0.770	−0.0393		
		3.0	0.289	0.716	−0.0264		
		3.3	0.252	0.667	−0.0166		
$_{48}Cd^{114}$	555	1.9	1.062	1.072	−0.151	0.9973	0.9871
		2.1	0.877	1.036	−0.132	0.9959	0.9846
		2.4	0.695	0.984	−0.108	0.9944	0.9770
		2.7	0.567	0.932	−0.0878	0.9931	0.9722
		3.0	0.476	0.881	−0.0712	0.9918	0.9668
		3.3	0.406	0.834	−0.0567	0.9888	0.9604
$_{78}Pt^{194}$	330	2.0	0.824	0.971	−0.104	0.9910	0.9739
		2.4	0.612	0.896	−0.0769	0.9868	0.9568
		2.5	0.575	0.873	−0.0692		
		2.7	0.508	0.839	−0.0587		
		3.0	0.428	0.794	−0.0458	0.9813	0.9288
		3.5	0.336	0.718	−0.0276		
		4.0	0.272	0.654	−0.0152	0.9731	0.8515
		4.5	0.227	0.594	−0.0050		
		5.0	0.192	0.541	+0.0027	0.9661	

[10] P. H. Stelson and F. K. McGowan, Phys. Rev. **99**, 112 (1955).
[11] M. E. Rose, Phys. Rev. **91**, 610 (1953).

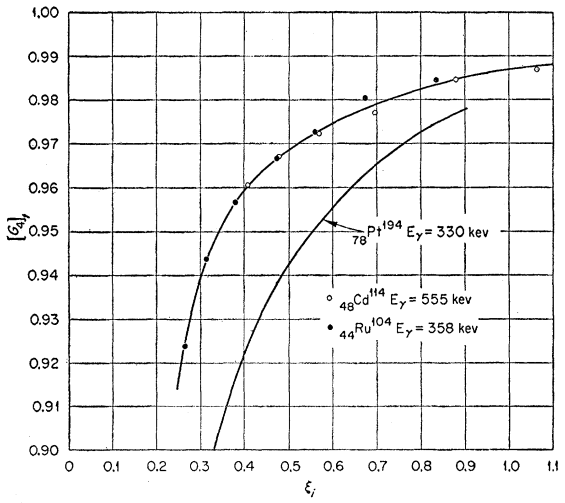

FIG. 5. The effective attenuation coefficient $[G_4]_t$ for multiple Rutherford scattering as a function of ξ_i for a few representative cases.

is similar with the exception that the intensities of the 358- and 403-kev gamma rays relative to the 330-kev gamma ray are reduced by factors of 9 and 39, respectively.

In Table II we tabulate $(a_\nu A_\nu)_{\text{exp}}$, which have been corrected for finite angular resolution,[11] and are defined as

$$(a_\nu A_\nu)_{\text{exp}} = \mathfrak{A}_\nu/\mathfrak{A}_0.$$

The errors quoted in Table II will be discussed in Sec. IV. Since the A_ν are known in the case of even-even nuclei, the particle parameters $(a_\nu)_{\text{exp}}$ for a thick target are determined and these are listed under columns 5 and 7 of Table II.

In Table III we list results from angular distribution measurements of other even-even nuclei which have not been studied as extensively as the four nuclei in Table II.

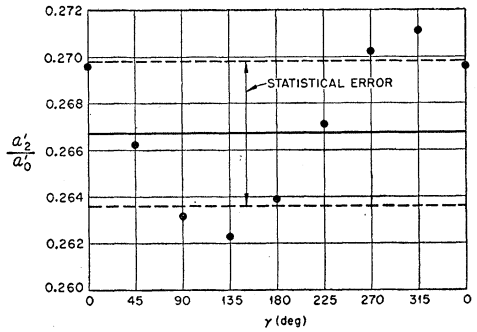

FIG. 6. The angular distribution coefficient $\mathfrak{A}_2'/\mathfrak{A}_0'$ as a function of γ. The solid line is the value of $\mathfrak{A}_2'/\mathfrak{A}_0'$ when target is assumed to be centered and the dashed lines represent the limits of error (standard deviation) to be expected from the finite number of counts collected in the experiment. The points represent the values of the $\mathfrak{A}_2'/\mathfrak{A}_0'$ for a displacement of the target along a direction making an angle γ with respect to the forward direction of the ion beam.

IV. INTERPRETATION AND DISCUSSION

In order to compare the particle parameters for a thick target as measured by experiment with those calculated from theory, we must evaluate the expected thick-target particle parameters. For an incident proton energy E_i in the laboratory system these particle parameters $[a_\nu]_t$ for a thick target are given by[4]

$$[a_\nu(E_i)]_t = \int_0^{E_i} \frac{\sigma(E)a_\nu dE}{dE/d\rho x} \Big/ \int_0^{E_i} \frac{\sigma(E)dE}{dE/d\rho x}, \qquad (3)$$

where $\sigma(E)$ is the total excitation cross section for electric quadrupole excitation and $dE/d\rho x$ is the rate of energy loss.[12] The integrals in Eq. (3) have been evaluated numerically using for a_ν the numerical results[5,7] obtained from a quantum-mechanical treatment of the Coulomb excitation process. These results are tabulated in Table IV under columns 5 and 6.

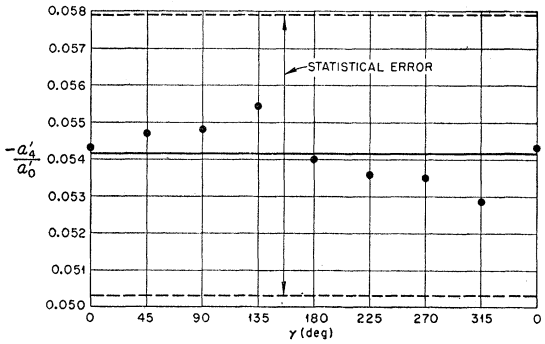

FIG. 7. The angular distribution coefficient $\mathfrak{A}_4'/\mathfrak{A}_0'$ as a function of γ. The solid line is the value of $\mathfrak{A}_4'/\mathfrak{A}_0'$ when target is assumed to be centered and the dashed lines represent the limits of error (standard deviation) to be expected from the finite number of counts collected in the experiment. The points represent the values of the $\mathfrak{A}_4'/\mathfrak{A}_0'$ for a displacement of the target along a direction making an angle γ with respect to the forward direction of the ion beam.

The slight attenuation of the angular distribution of the gamma rays by the multiple scattering of the protons by Rutherford scattering as they traverse a thick target has been discussed in a previous paper.[4] The form of the correlation function is unchanged and each coefficient $a_\nu A_\nu$ becomes multiplied by an attenuation factor G_ν. Following the notation of Goudsmit and Saunderson,[13] who have expressed the multiple scattering function as a series in Legendre polynomials, the G_ν are given by

$$G_\nu = e^{-x_\nu}, \qquad (4)$$

where

$$x_\nu = 2\pi K^2 N t \nu(\nu+1)[\log\beta - (\tfrac{1}{2}+\tfrac{1}{3}+\cdots 1/\nu)].$$

The reader is referred to their treatment for a discussion of the assumptions inherent in Eq. (4). In our previous

[12] We will send to those who are interested the values we have taken for $dE/d\rho x$ for protons.

[13] S. Goudsmit and J. L. Saunderson, Phys. Rev. **57**, 24 (1940).

paper[4] we chose for the effect of screening by the atomic electrons a cutoff in the Rutherford scattering law which was not appropriate for the scattering of protons.[14] The effect of the cutoff comes into the attenuation coefficient through the factor $\log\beta$. According to Williams[15] the Born approximation is not valid for $\eta_i \equiv Ze^2/\hbar v_i \gg 1$ but instead one must use the classical method of orbits in the treatment of multiple scattering with shielding. For our experiments we have $4 \leq \eta_i \leq 11$ and we have chosen a cutoff which Williams found appropriate to fit some data from multiple scattering of α particles. In addition the values of $dE/d\rho x$ have been revised upward by 8 to 10%. The net result of these changes is to reduce the x_ν about 40%. The effective attenuation coefficients $[G_\nu]_t$ for a thick target have been evaluated for a few cases, where $[G_\nu]_t$ is defined by

$$[G_\nu]_t = \int_0^{E_i} \frac{\sigma(E) a_\nu G_\nu dE}{dE/d\rho x} \Big/ \int_0^{E_i} \frac{\sigma(E) a_\nu dE}{dE/d\rho x}, \qquad (5)$$

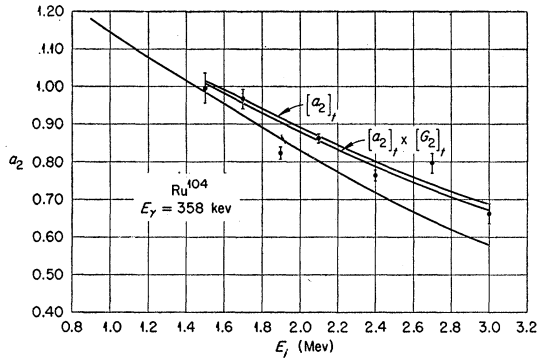

FIG. 8. Particle parameter a_2 as a function of the incident proton energy for Ru^{104}.

and G_ν is given by Eq. (4). These results are listed in Table IV under columns 7 and 8. Since the effect of multiple Rutherford scattering on the angular distribution coefficients is relatively small, we have not computed the $[G_\nu]_t$ for every entry in Table IV. For neighboring nuclei we find that $[G_\nu]_t$ fall on a smooth curve as a function of ξ_i, where

$$\xi = \frac{Z_1 Z_2 e^2}{\hbar}\left(\frac{1}{v_f} - \frac{1}{v_i}\right).$$

The curves in Figs. 4 and 5 were used to obtain $[G_\nu]_t$ for the other entries in Table IV.

The errors quoted in Table II include both the standard deviation to be expected on purely statistical grounds from the finite number of counts collected in the experiments and the standard deviation to be

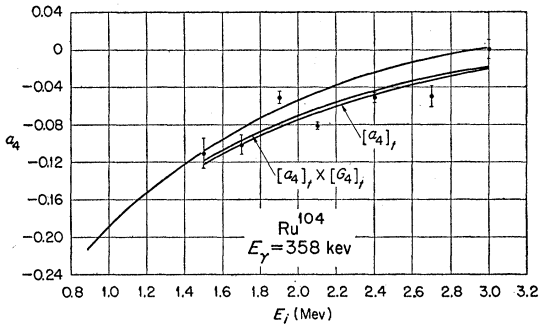

FIG. 9. Particle parameter a_4 as a function of the incident proton energy for Ru^{104}.

expected from the uncertainty in the alignment of the axis of rotation (decentering error). The decentering error was estimated as follows. Breitenberger has given relations[16] to calculate the total first-order counting error as a function of source displacement for any given correlation function. For example, the total first-order counting errors were calculated for a source displacement $d = 0.05/20 = 0.0025$ which is likely to arise in our apparatus. These counting rate errors were applied to data obtained from Ru^{104} for $E_p = 2.4$ Mev. For each displacement a least-squares fit to the modified counting rates or intensities was made to determine the coefficients $\mathfrak{A}_\nu'/\mathfrak{A}_0'$. The results are given in Figs. 6 and 7. The solid line in each figure is the value of $\mathfrak{A}_\nu'/\mathfrak{A}_0'$ for the case when the source or target is assumed to be centered and the dashed lines represent the limits of error (standard deviation) to be expected from the finite number of counts collected in the experiment. In this experiment 5×10^4 counts were collected at each of the 10 angles. The points represent the values of the coefficients $\mathfrak{A}_\nu'/\mathfrak{A}_0'$ as a function of the displacement of the target along a direction making an angle γ with respect to the forward direction of the ion beam. For this particular example the error introduced in $\mathfrak{A}_2'/\mathfrak{A}_0'$

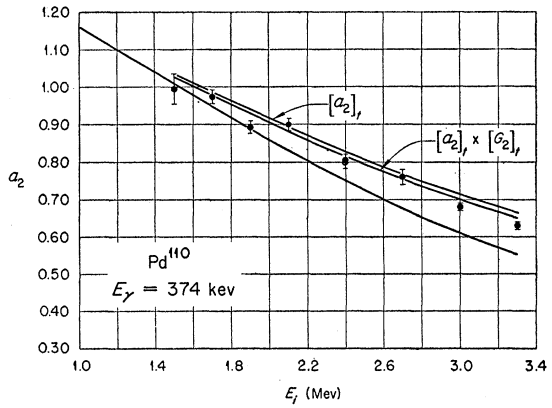

FIG. 10. Particle parameter a_2 as a function of the incident proton energy for Pd^{110}.

[14] We are indebted to Dr. T. Huus (private communication) for pointing out that the attenuation appeared to be too large in our previous paper.

[15] E. J. Williams, Phys. Rev. 58, 292 (1940).

[16] E. Breitenberger, Phil. Mag. 45, 497 (1954).

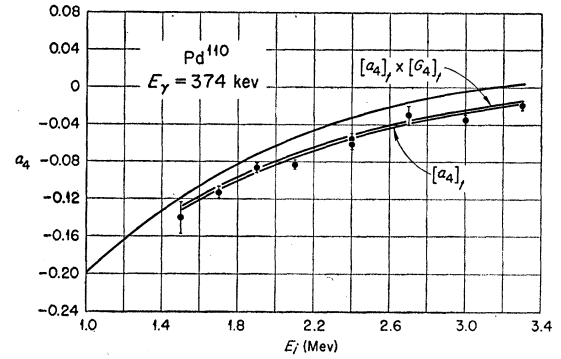

FIG. 11. Particle parameter a_4 as a function of the incident proton energy for Pd^{110}.

from target displacement can be as large as the statistical error while the error introduced in $\mathfrak{A}_4'/\mathfrak{A}_0'$ is considerably smaller for all displacements. Unfortunately the displacement at $\gamma=135°$ or 315° is the one most likely to occur in our apparatus. As a result we have combined a decentering error of 0.003 and 0.001 for $(a_2A_2)_{\text{exp}}$ and $(a_4A_4)_{\text{exp}}$, respectively, with the statistical error by taking the square root of the sum of the squares of these two standard deviations.

A comparison between experiment and theory using the particle parameters obtained from the quantum-mechanical treatment is shown in Figs. 8 to 15. The solid curve (not labeled) is a_ν as a function of E_i, the incident energy of the proton. The thick-target particle parameter as a function of E_i is labeled $[a_\nu]_t$. Finally, the curve labeled $[a_\nu]_t \times [G_\nu]_t$ is the expected thick-target particle parameter including a correction for multiple scattering of the protons as they traverse the target. It is this latter curve that is to be compared with the experimental points. For example, in the case of Cd^{114} the yield changes by a factor of 200 in going from 1.9 to 3.3 Mev. We conclude to within the accuracy of the experiments (±2 to 5% for a_2) that there is agreement between experiment and the numerical results from the exact treatment of the process. In the range of interest ($4 \leq \eta_i \leq 11$), the semiclassical results are 10 to 20% smaller than the quantum-mechanical results for a_2.

In the discussion thus far we have neglected the effect of any possible Coulomb excitation of other states in these even-even nuclei. For example, a spin 2 is consistent with the directional angular correlation measurements[17] for the second excited state (622 kev) in Pt^{194}. In principle this state could be excited by Coulomb excitation either by direct excitation 0→2 or by double $E2$ excitation 0→2→2. The cross section for double $E2$ excitation is given approximately by[18]

$$\sigma_{0\to2\to2} = \sigma_{0\to2}\sigma_{2\to2}/d^2,$$

where d is the distance of closest approach. If we assume $B(E2)_d$ for the 292-kev cascade transition to be equal to 0.39×10^{-48} cm^4, the $B(E2)_d$ for the 330-kev transition,[10] then $\sigma_{0\to2\to2}$ is 1.12 μb at $E_p=5.0$ Mev. For direct excitation of the 2+ level at 622 kev, the cross section is 50 μb on the assumption that the $B(E2)_d = B(E2)_{sp} = 6.67\times10^{-51}$ cm^4. The observed cross section for excitation of the 330 kev state is 5.2 mb. These estimates are sufficient to exclude any significant excitation of other states in these even-even nuclei. As a result the angular distribution measurements should not contain any contributions from cascade transitions. We have, however, made a few preliminary measurements in an attempt to observe excitation of other 2+ and 4+ levels either by double $E2$ excitation or by direct excitation in the case of 2+ levels. The results verify the conclusion that the angular distribution measurements are free of any effect from cascade transitions. The number of excitations for the 622-kev state in Pt^{194} does, however, have some significance with regard to the reduced transition probabilities from the second excited 2+ state to the first 2+ state and to the ground state. We observed excitation of the 622-kev state by detecting the 292-kev gamma ray in coincidence with the 330-kev gamma ray. From the coincidence spectrum we find $(4.96\pm0.75)\times10^3$ excitations

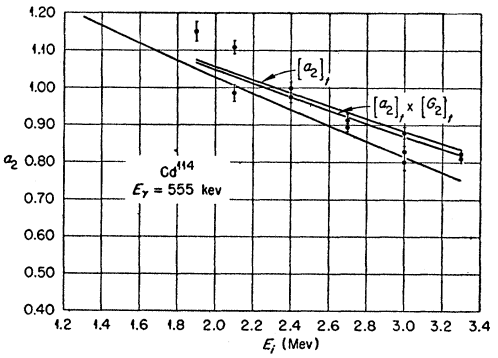

FIG. 12. Particle parameter a_2 as a function of the incident proton energy for Cd^{114}.

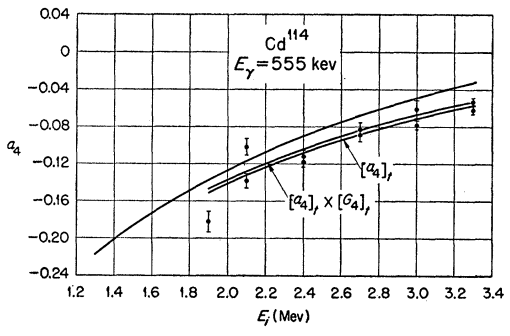

FIG. 13. Particle parameter a_4 as a function of the incident proton energy for Cd^{114}.

[17] Mandeville, Varma, and Saraf, Phys. Rev. 98, 94 (1955).
[18] A. Winther (private communication); Alder, Bohr, Huus, and Winther, Revs. Modern Phys. 28, 432 (1956).

per microcoulomb for the 622-kev state by 5-Mev protons on a thick target with abundance of Pt^{194} of 65%. The $B(E2)_d$ for the 622-kev transition is $(1.74 \pm 0.35) \times 10^{-51}$ cm^4, which is $\frac{1}{4}$ of the $B(E2)_{sp}$. Using the branching ratio[19] 3.3 for cascade transitions to crossover transitions and assuming the 292-kev transition is predominantly $E2$, which is in accord with observations[20] for the analogous transition in Pt^{196}, we we find the $B(E2)_d$ for the 292-kev transition is 2.31×10^{-49} cm^4. This result is 35 times $B(E2)_{sp}$, while $B(E2)_d/B(E2)_{sp}$ is 58 for the 330-kev transition. In these results the yield has been attributed to direct excitation of the 622-kev state because the cross section for double $E2$ excitation is much smaller. This result, *viz.*, that the $B(E2)_d$ for the 2→2 transition is smaller than the $B(E2)_d$ for the 2→0 transition, is of some interest. It is in contradiction to the predictions of both the "shape unstable" model[21] and the "free vibration" model[22] which predict that the $B(E2)_d$ for the 2→2 transition should be larger than the $B(E2)_d$ for the 2→0 transition of 330 kev.

We have found it useful to plot $[a_\nu]_i \times [G_\nu]_i$ as a function of ξ_i for interpolation purposes rather than compute the thick-target particle parameters for every case when they are needed. These curves will appear in a subsequent paper along with a few additional thick-target parameters which have been computed for several cases to interpret angular distribution measurements from odd-mass nuclei.

The results given in Table III for measurements from other even-even nuclei indicate that, as expected, the spin of the Coulomb excited state is 2. The errors

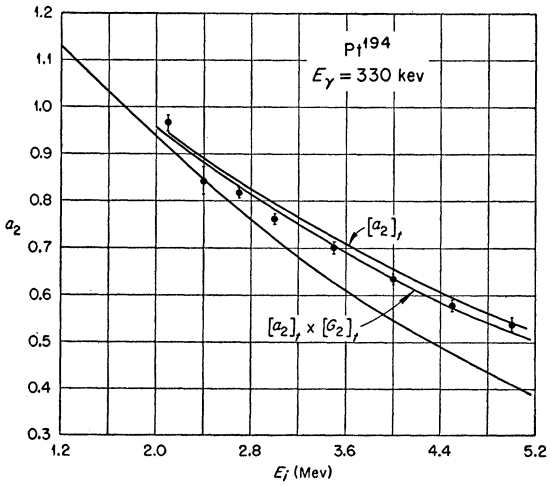

FIG. 14. Particle parameter a_2 as a function of the incident proton energy for Pt^{194}.

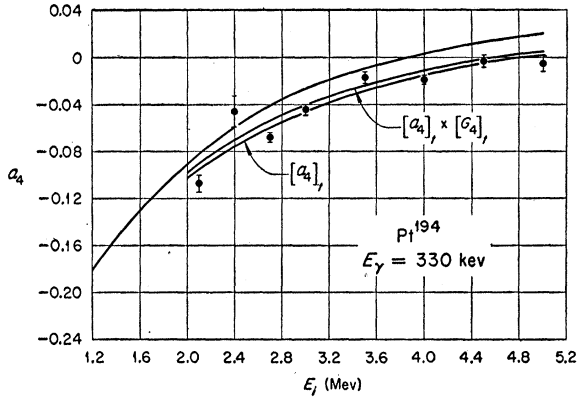

FIG. 15. Particle parameter a_4 as a function of the incident proton energy for Pt^{194}.

assigned to these results are larger than those in Table II. The Pd^{108} target contained a small amount Na^{23} as an impurity which gave rise to a gamma ray at 440 kev with an intensity of about 4% relative to the 433-kev gamma ray from Pd^{108}. The isotopic abundance of the enriched cadmium targets was not too large. As a result the contribution of the other isotopes in the targets to angular distributions had to be removed from the composite data.

V. CONCLUSIONS

The particle parameters a_ν for a thick target which appear in the distribution function for the directional correlation of gamma rays following Coulomb excitation have been measured in the even-even nuclei Ru^{104}, Pd^{110}, Cd^{114}, and Pt^{194} and no significant deviation from the numerical results given by quantum-mechanical treatment is found. The good agreement between theory and experiment is encouraging for the use of Coulomb excitation as a valuable tool in nuclear spectroscopy.

For mixed $E2+M1$ transitions, such as are generally observed in odd-mass nuclei, a measurement of the angular correlation affords a sensitive means of determining the ratio $(E2/M1)^{\frac{1}{2}}$, in addition to inferring the spins of the excited states. This information combined with the cross section for excitation yields the reduced transition probability for the magnetic dipole transition. Measurements of this type combined with the polarization-direction correlation to eliminate ambiguities will be discussed in a subsequent paper on odd-mass nuclei.

It is a pleasure to express our appreciation to Professor L. C. Biedenharn and Professor G. Breit for stimulating discussions concerning the results. We should like to express appreciation to Buford Carter who carried out the I.B.M. calculations. We wish to acknowledge the participation of Dr. M. M. Bretscher, a research participant for the summer of 1955 from Alabama Polytechnic Institute, in some of these measurements.

[19] M. W. Johns and S. V. Nablo, Phys. Rev. **96**, 1599 (1954).
[20] R. M. Steffen, Phys. Rev. **89**, 665 (1953).
[21] L. Wilets and M. Jean, Phys. Rev. **102**, 788 (1956).
[22] G. Scharff-Goldhaber and J. Weneser, Phys. Rev. **98**, 212 (1955).